Current Density versus Potential Characteristics of Dye-Sensitized Nanostructured Semiconductor Photoelectrodes. 2. Simulations

Jae-Joon Lee,[†,§] George M. Coia,[*,‡] and Nathan S. Lewis[*,†]

Noyes Laboratory, 127-72, Division of Chemistry and Chemical Engineering, California Institute of Technology, Pasadena, California 91125, and Department of Chemistry, Portland State University, P.O. Box 751, Portland, Oregon 97207

Received: May 2, 2003; In Final Form: September 25, 2003

The impact of changes in various parameters on the steady-state current density−potential ($J-E$) characteristics of dye-sensitized nanostructured semiconductor photoelectrodes has been evaluated through a series of simulations. The model parameters can be divided into three classes, designated as type I, type II, and type III, respectively. Type I parameters primarily affect the open-circuit potential without changing the overall shape of the $J-E$ curves. Type II parameters primarily affect the limiting quantum yield for photocurrent production. Rate constants for injection and quenching of the excited state of the dye by the contacting phase are type II parameters, whereas the rate constant for the direct electrolyte reduction reaction, the reduced equilibrium constant for iodine formation, and the rate constant for recombination are type I parameters. The rate constant for regeneration affects both the shape of the $J-E$ curves and the limiting quantum yield for photocurrent flow, and it is therefore designated as a type III parameter. Variation of the diffusion coefficient parameter for electrons in the semiconducting membrane produces a mixed response having both type I and II characteristics. Comparisons between simulations and experimental data have delineated the factors that should be manipulated to increase the energy conversion efficiency of photoelectrochemical cells that utilize nanostructured TiO_2 electrodes.

I. Introduction

The preceding manuscript presented a set of differential equations and associated boundary conditions that collectively comprise a closed-form analytical description of the rate processes in a dye-sensitized nanocrystalline photoelectrode.[1] This manuscript presents simulations using the resulting model with various values of input parameters. Of specific interest are the effects of changing the charge-carrier mobility in the TiO_2 membrane or of changing the rate constants for injection, recombination, or regeneration of the oxidized dye species. The simulations additionally reveal scenarios in which low values of the limiting photocurrent quantum yield are produced by dyes that rapidly inject electrons into the semiconductor membrane.

The working model expressions enable the calculation of current density−potential ($J-E$) characteristics for sandwich type cells in which the counter electrode is separated from the photoelectrode by a spacer of arbitrary thickness. However, the plots presented herein correspond to the simpler case in which the concentrations of the redox species at the edge of the membrane ($X = 1$) are fixed at their bulk values. Such is the case when the photoelectrode is immersed in an ample volume of stirred electrolyte solution. The effect of concentration polarization at the counter electrode in sandwich type cells has been treated elsewhere.[2]

Table 1 lists the parameters that were held constant for the numerical calculations performed in this work, unless otherwise specified. Typical concentrations of redox species in the electrolyte phase are $[I_3^-] = 0.05$ M and $[I^-] = 0.50$ M, leading to values of $\mathbf{P}_c(1) = 0.1$ and $\mathbf{N}_c(1) = 0.5$, respectively.[3] The diffusion coefficients of these species in CH_3CN are estimated to be $\sim 2 \times 10^{-5}$ cm^2 s^{-1} or smaller.[4] Diffusion coefficients of species confined to the pores of nanostructured TiO_2 are reported to decrease by a factor no greater than the porosity of the medium,[5] and the membane was assumed to consist of 15−20 nm TiO_2 nanoparticles packed in a cubic lattice, yielding a volume-to-surface ratio, L, of $\sim 1.0 \times 10^{-6}$ cm. Assuming that the membrane is 10 μm in thickness ($\delta = 10^{-3}$ cm), $\Psi_0 \approx 1.0 \times 10^{17}$ cm^{-2} s^{-1},[6] and $p_c^\circ = n_c^\circ = 1.0 \times 10^{-3}$ mol cm^{-3}, which implies $\mathbf{D}_{p_c} = \mathbf{D}_{n_c} = 50$. In simulations where the low-intensity approximation was invoked, $\mathbf{A}$ (eq A.3.11 in Appendix III in the preceding manuscript) was set equal to 5 (i.e., $\alpha = 5.0 \times 10^3$ cm^{-1}), corresponding to extinction of ~99% of the incident light, and β (eq 11 in the preceding manuscript) was set equal to 1, indicating that all extinction is due to the dye. In simulations where the low-intensity approximation was not invoked, $\mathbf{e}_d$ was set equal to 5 and all other extinction coefficients were set equal to zero. (Both conditions are mutually equivalent and correspond to $\epsilon_d \approx 2.0 \times 10^{-17}$ cm^2 when the dye coverage is $\sim 1.0 \times 10^{14}$ cm^{-2}. Similar values have been found in the literature.[2,7])

The conventional TiO_2/Ru(4,4′-dicarboxylic acid 2,2′-bipyridine)$_2$(NCS)$_2$ system operates far from equilibrium because the energetics of the key rate processes highly favor injection, recombination, and regeneration relative to the rates of the microscopic reverse reactions for these specific processes. The R factors (R_{ij}) for injection and recombination were therefore set to zero, but the R factor for regeneration was solved for on the basis of the difference between the Nernstian potential

* To whom correspondence should be addressed. Phone: +1 503 725 5861. Fax: +1 503 725 3888. E-mail: coia@pdx.edu (GMC). Phone: +1 626 395 6335. Fax: +1 626 795 7487. E-mail: nslewis@caltech.edu (NSL).
† California Institute of Technology.
‡ Portland State University.
§ Present address: Department of Applied Chemistry, Konkuk University, Chungju, Korea.

10.1021/jp035195m CCC: $27.50
Published on Web 04/08/2004

TABLE 1: Constants and Parameters for Simulation

description	original variable	dimensionless eq	ref eq no.[a]
concentration of charge carriers	$p_c(\delta) = [I_3^-] = 0.05$ M	$\mathbf{P}_c(1) = 0.1$	eq D.1.3
	$n_c(\delta) = [I^-] = 0.5$ M	$\mathbf{N}_c(1) = 0.5$	eq D.1.4
constants	α ($=e_d d$) $= 5.0 \times 10^3$ cm^{-1}	$\mathbf{A} = 5$, $\beta = 1$	eqs A.3.11 and 11
	$\epsilon_d = 2.0 \times 10^{-17}$ cm^2	or	
	$\epsilon_{n_s} = \epsilon_{n_c} = \epsilon_{p_c} = 0$	$\mathbf{e}_d = 5$,	
	$d_0 = 1.0 \times 10^{14}$ cm^{-2}	$\mathbf{e}_{n_s} = \mathbf{e}_{n_c} = \mathbf{e}_{p_c} = 0$	eq D.4.5
diffusion coefficients	$D_{n_s} \approx 2.3 \times 10^{-5}$ cm^2 s^{-1}	$\mathbf{D}_{n_s} = 1$	eq D.2.1
	$D_{p_c} = D_{n_c} \approx 1.0 \times 10^{-5}$ cm^2 s^{-1}	$\mathbf{D}_{p_c} = \mathbf{D}_{n_c} = 50$	eqs D.2.2 and D.2.3
baseline scenario	$k_{d^*s} \approx 10^{12}$ to 10^{13} s^{-1}	$\mathbf{k}_{d^*s} = 1.0 \times 10^5$	eqs D.3.1−D.3.6
	$k_{sc} \approx 6.0 \times 10^{-27}$ cm^4 s^{-1}	$\mathbf{k}_{sc} = 1.0 \times 10^{-5}$	
	$k_{cd} \approx 4.0 \times 10^{-15}$ cm^3 s^{-1}	$\mathbf{k}_{cd} = 1.0 \times 10^3$	
	($k'_{cd} \sim 1.0 \times 10^6$ s^{-1})		
	$k_{sd} \approx 10^{-13}$ to 10^{-12} cm^3 s^{-1}	$\mathbf{k}_{sd} = 10$	
	$k_{d^*c} = k_{oc} = 0$	$\mathbf{k}_{d^*c} = \mathbf{k}_{oc} = 0$	
	$k_d = 1.7 \times 10^7$ s^{-1}		
	$[K_I/(p_c^\circ n_c^\circ)]^{1/2} = 1$, $f = 4.5$, $\phi_s = 1$		

[a] See the preceding manuscript.[1]

of the adsorbed dye$^{+/0}$ system and the Nernstian potential of the redox active species in the electrolyte. The rate constant relationships derived in the previous manusript have been used to ensure self-consistency in the modeling effort. However, instead of treating an individual system by choosing specific values of the reorganization energy and electronic coupling parameters, we present simulations for a wide range of possible cases, with the rate constants as input parameters, to explore the effects that changes in various chemical and physical parameters of interest will have on the $J-E$ properties of the photoelectrode.

II. Methods

The boundary value problem described in the previous manuscript was solved by numerical integration using the fourth-order Runge−Kutta method.[8] The functions $\mathbf{N}_s(X)$, $\mathbf{P}_c(X)$, $\mathbf{N}_c(X)$, and $\int_0^X \mathbf{P}_d(U)\,dU$ were solved for, and because the first three functions are defined in terms of their second derivatives, the first derivatives $\mathbf{N}'_s(X)$, $\mathbf{P}'_c(X)$, and $\mathbf{N}'_c(X)$ were also obtained. Initial ($X = 0$) values for $\mathbf{N}_s(X)$ and $\int_0^X \mathbf{P}_d(U)\,dU$ were obtained directly from the boundary conditions, while the remaining boundary values were arrived at iteratively, starting with estimated initial values. For solutions computed in the low-intensity limit, the number of differential equations is reduced by one, as $\mathbf{P}_d$ is given by an analytical expression (eq A.3.15 in Appendix III in the preceding manuscript). Current density−potential ($J-E$) characteristics were simulated by solving the boundary value problem for a range of applied bias.

III. Results

A. "Baseline Scenario". The effects of the various model input parameters on the calculated current density versus potential characteristics are discussed in this section. A "baseline" case is developed, and changes in the $J-E$ behavior are then examined as each parameter of interest is varied individually.

Figure 1 displays the $J-E$ curve calculated for a set of parameters that are representative of current experimental best estimates for the TiO_2/Ru(4,4′-dicarboxylic acid 2,2′-bipyridine)$_2$-$(NCS)_2$−CH_3CN−I_3^-−I^- system. The value of $\mathbf{D}_{n_s}$ was set to 1, which corresponds to a diffusion coefficient of electrons (D_{n_s}) of $\sim 2.0 \times 10^{-5}$ cm^2 s^{-1} when the equilibrium concentration of electrons in the dark ($n_{s,eq}$) is $\sim 10^{17}$ cm^{-3}. No quenching loss of the excited state of the dye by the contacting phase ($k_{d^*c} = 0$) is assumed, and the injection efficiency is therefore unity

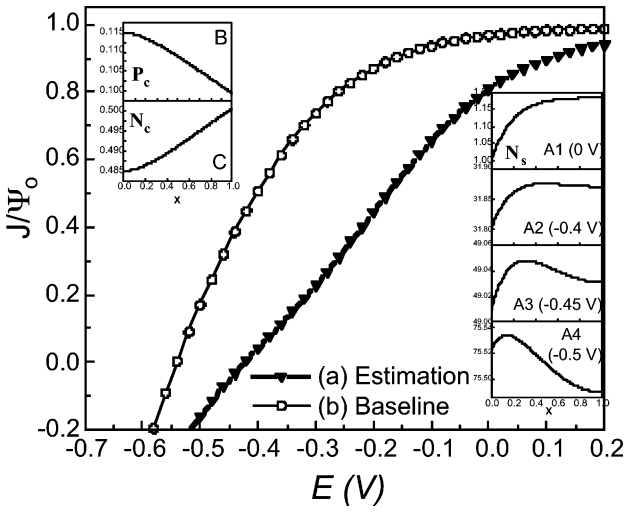

Figure 1. (a) $J-E$ curve calculated for a set of parameters that are representative of the best current experimental estimates for the TiO_2/Ru(4,4′-dicarboxylic acid 2,2′-bipyridine)$_2$(NCS)$_2$ CH_3CN−I_3^-−I^- system: $\mathbf{k}_{d^*s} = 1.0 \times 10^5$, $\mathbf{k}_{sc} = 1.0 \times 10^{-5}$, $\mathbf{k}_{cd} = 1.0 \times 10^2$, $\mathbf{k}_{sd} = 10$. The simulation was performed under the low-intensity limit, it was assumed that there is no quenching loss of the excited state of the dyes by the contacting phase ($\mathbf{k}_{d^*c} = 0$), and the other parameters used were $\phi_s = 1$, $f = 4.5$, and $[K_I/(p_c^\circ n_c^\circ)]^{1/2} = 1$. All other parameters are the same as those in Table 1. (b) The $J-E$ curve corresponds to the baseline scenario which consists of the best set of parameters with which the resulting simulation is in good accord with the experimental observations as close as possible with no inflection point. The parameters for the baseline scenario are identical to those in part a except that $\mathbf{k}_{cd}$ is set to 1.0×10^3. Other parameters are as described in the text and Table 1. (c, insets): A1−A4, concentration profiles for electrons in the semiconductor ($\mathbf{N}_s$) are calculated for $E = 0$, −0.4, −0.45, and −0.50 V, respectively; B and C, concentration profiles for charge carriers in the membrane at $E = 0$ V.

($\phi_s = 1$). This is a reasonable approximation given that electron injection (k_{d^*s}) proceeds largely on ultrafast time scales (10^{12} to 10^{13} s^{-1}), which corresponds to $\mathbf{k}_{d^*s} \approx 1.0 \times 10^5$.[9,10] The rate constant for regeneration of the oxidized dye (k_{cd}) was taken to be 4.0×10^{-16} cm^3 s^{-1} ($\mathbf{k}_{cd} = 1.0 \times 10^2$), which corresponds to a pseudo-first-order rate constant ($k'_{cd} = k_{cd}[I^-]$) of $\sim 1.0 \times 10^5$ s^{-1} when $[I^-] = 0.5$ M.[7] A moderate value of the direct-reduction rate constant from the semiconductor to the electrolyte (k_{sc}) has been assumed, with $\mathbf{k}_{sc} = 1.0 \times 10^{-5}$ and $[K_I/(p_c^\circ n_c^\circ)]^{1/2} = 1$, where $[K_I/(p_c^\circ n_c^\circ)]^{1/2}$ is the reduced equilibrium constant for iodine formation. The quality factor (f) was 4.5, in accord with experimental measurements.[11] Rate constants for

recombination $\mathbf{k}_{sd} = 10$ ($k_{sd} \approx 10^{-13}$ to 10^{-12} cm^3 s^{-1}) were derived from experimental measurements.[7]

The calculation was performed using the simplified model applicable in the low-intensity limit. In general, essentially no difference was observed between the simulations using either the general case or the low-intensity limit. Therefore, unless otherwise specified, the low-intensity assumption was applied in the simulations below.

As shown in the figure, the resulting simulation (filled down-triangles) does not closely resemble the measured $J-E$ behavior of the TiO_2/Ru(4,4′-dicarboxylic acid 2,2′-bipyridine)$_2$(NCS)$_2$−$CH_3CN-I_3^-$−I^- system. An inflection point is observed in the simulation whereas none is observed experimentally, and the simulated open-circuit voltage is significantly smaller than the observed value.[12] Examination of the simulation results reveals that the rate of recombination has been overestimated and/or the rate of regeneration has been underestimated. As a consequence, for $E > -0.6$ V, the light-generated component of the current is less than what is observed experimentally.

Figure 1 therefore depicts a second simulation (open circles) in which the value of the regeneration rate constant has been increased to $k_{cd} = \sim 4.0 \times 10^{-15}$ cm^3 s^{-1} ($\mathbf{k}_{cd} = 1.0 \times 10^3$). The resulting simulation is in good accord with the experimental observations. Consequently, this parameter set was selected as the "baseline scenario" (Table 1).

The insets of Figure 1 display the computed concentration profiles of charge carriers in the semiconductor ($\mathbf{N}_{s'}$ A1−A4) and in the electrolyte portions of the membrane ($\mathbf{P}_c$ and $\mathbf{N}_c$ for B and C, respectively) at various biases (E) in the baseline scenario. At low bias (A1), the electron concentration decreases monotonically from the outer boundary of the membrane ($X = 1$) to the current-collecting contact ($X = 0$, semiconductor/substrate interface). Under these conditions, diffusion along the concentration gradient provides near-unit collection efficiency. However, as the bias becomes more negative, a peak in the electron concentration profile, $\mathbf{N}_s(X)$, appears near the current-collecting contact (A2−A4). This indicates that when the bias is sufficiently negative, electrons generated deeper in the semiconductor membrane will diffuse away from the current-collecting contact and will recombine with I_3^-.

The situation under these conditions is somewhat different for the other charge carriers in the system. The magnitude of any charge-carrier concentration gradient is controlled by the ratio of the corresponding diffusion coefficient to the incident flux. Using the values for $\mathbf{D}_{p_c}$ and $\mathbf{D}_{n_c}$ estimated above, the concentration gradients for $\mathbf{P}_c$ and $\mathbf{N}_c$ are found to be relatively small. Hence, unlike the concentration gradient of the electrons, the concentration gradients for $\mathbf{P}_c$ and $\mathbf{N}_c$ do not vary significantly with changes in bias.

B. Variation in the Diode Quality Factor, *f*. Figure 2 shows the effects of changes in the model parameter f. This empirical parameter describes how the concentration of electrons at the current-collecting contact changes with applied bias (eq 16 in the preceding manuscript). With $f = 1$, the $J-E$ characteristics approach ideal diode behavior, with the direct-reduction current increasing by a factor of 10 for every 59 mV decrease in bias. Larger values of f cause the current to change more gradually as a function of the applied bias. In the remaining simulations, f was set to 4.5, an experimentally derived value.[11]

C. Effect of Varying the Direct-Reduction Rate Constant, $\mathbf{k}_{sc}$, and the Reduced Equilibrium Constant, $[K_I/(p_c^\circ n_c^\circ)]^{1/2}$. Figures 3 and 4 depict the effects of varying the dimensionless direct-reduction rate constant, $\mathbf{k}_{sc}$, and the model parameter, $[K_I/(p_c^\circ n_c^\circ)]^{1/2}$, respectively. The latter is directly proportional to the concentration of the electron acceptor, [I], in the electrolyte, for the specific equilibria used in the $J-E$ model being evaluated.[1]

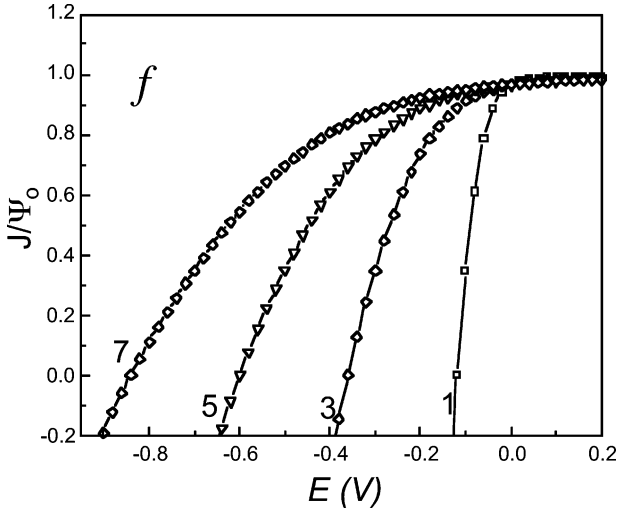

Figure 2. $J-E$ characteristics at different values of the quality factor, f. Calculations are in the low-intensity limit, and $\phi_s = 1$. Labels correspond to values of f. Other parameters are the same as those in Figure 1.

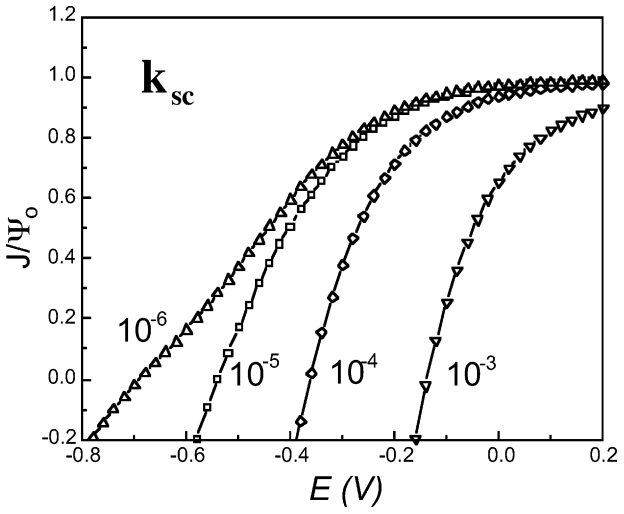

Figure 3. $J-E$ characteristics at different values of the direct-reduction rate constant parameter ($\mathbf{k}_{sc}$). Calculations are in the low-intensity limit, and $\phi_s = 1$. Labels correspond to values of $\mathbf{k}_{sc}$. Other parameters are the same as those in Figure 1.

Changes in both parameters greatly affect the $J-E$ behavior. The open-circuit potential shifts by more than 200 mV per order of magnitude change in each parameter, but the overall shape of the $J-E$ curves is retained as the values are increased above some lower-bound limit. The $J-E$ curve shifts positively because the direct-reduction rate increases as a result of either increasing $\mathbf{k}_{sc}$ or increasing the concentration of the electron acceptor, [I]. At very small values of $\mathbf{k}_{sc}$ and/or $[K_I/(p_c^\circ n_c^\circ)]^{1/2}$, the direct-reduction current is insignificant and $J-E$ curves at very negative bias are dominated by the potential dependence of the light-induced portion of the current (cf. Figure 5, open symbols). Thus, decreases in the direct-reduction current in this range of potential produce relatively little shift in the anodic portion of the resulting $J-E$ curves.

The values of these two parameters cannot be separately deduced by fitting the experimental $J-E$ data, because $\mathbf{k}_{sc}$ and $[K_I/(p_c^\circ n_c^\circ)]^{1/2}$ are coupled. Assuming $[K_I/(p_c^\circ n_c^\circ)]^{1/2} = 1$, the best fit of $\mathbf{k}_{sc}$ to produce an open-circuit voltage (V_{oc}) of ~ -0.5 to

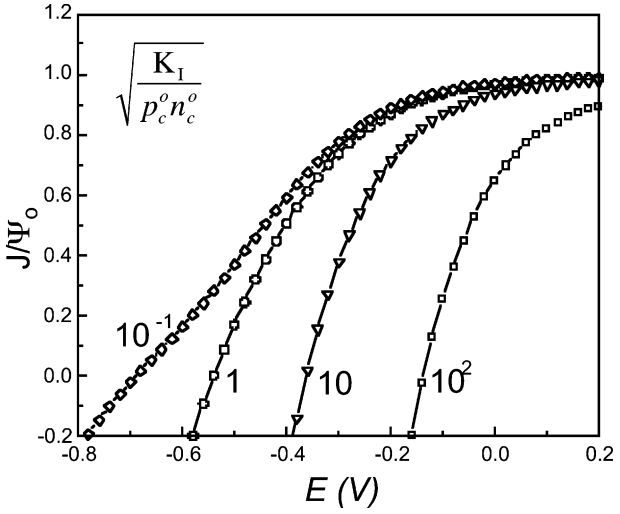

Figure 4. $J-E$ characteristics at different values of $[K_I/(p_c^o n_c^o)]^{1/2}$, calculated in the low-intensity limit and with $\phi_s = 1$. Labels correspond to the value of $[K_I/(p_c^o n_c^o)]^{1/2}$. Other parameters are the same as those in Figure 1 unless stated otherwise in the text.

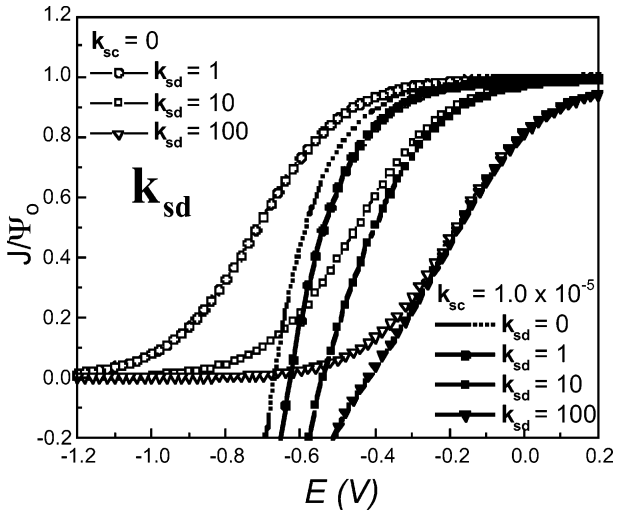

Figure 5. $J-E$ characteristics at various values of the recombination rate constant parameter ($\mathbf{k}_{sd}$), calculated in the low-intensity limit and with $\phi_s = 1$ when the regeneration rate constant parameter ($\mathbf{k}_{cd}$) is set to 1.0×10^3. Other parameters are the same as those in Figure 1. Curves with open symbols represent the $J-E$ characteristics when $\mathbf{k}_{sc} = 0$, while those with filled symbols display the corresponding $J-E$ curves with $\mathbf{k}_{sc} = 1.0 \times 10^{-5}$. The curve depicted by the dotted line represents the limiting case of no recombination ($\mathbf{k}_{sd} = 0$) with a nonzero direct-reduction rate ($\mathbf{k}_{sc} = 1.0 \times 10^{-5}$). The curve with filled squares corresponds to the baseline scenario shown in Figure 1 (open circles) and Table 1.

-0.6 V is $\mathbf{k}_{sc} \approx 1.0 \times 10^{-5}$, which corresponds to a rate constant for reaction between electrons in the semiconductor membrane and iodine in the solution of $k_{sc} \approx 6.0 \times 10^{-27}$ cm^4 s^{-1}.

D. Effects of Varying the Rate Constant for Recombination (k_{sd}). Figure 5 depicts the effects of varying the rate constant for recombination, k_{sd}, arising from reaction of the oxidized dye with electrons in the semiconductor. To compare this recombination process with the direct-reduction process arising from transfer of electrons in the semiconductor to the oxidized form of the redox species in the solution (with rate constant k_{sc}), two sets of simulations are depicted. One set (curves with open symbols) represents the $J-E$ characteristics calculated at different values of k_{sd} for the situation in which the solution-derived direct-reduction rate constant is set to zero ($k_{sc} = 0$), whereas the other set of curves (filled symbols) corresponds to the identical simulations but with the direct-reduction rate constant parameter set to $\mathbf{k}_{sc} = 1.0 \times 10^{-5}$ ($k_{sc} \approx 6.0 \times 10^{-27}$ cm^4 s^{-1}). The former condition could in principle be obtained by formation of a blocking layer on the exposed TiO_2 surface that allows dye regeneration but prevents direct reduction of the oxidized species in the electrolyte by electrons in the TiO_2.[13] The latter condition, in contrast, is representative of an actual photoelectrode in which cathodic direct-reduction current flows under forward bias conditions.

The competition between recombination (k_{sd}) and regeneration (k_{cd}) is most clearly seen when $\mathbf{k}_{sc} = 0$. The light-induced component of the current asymptotically approaches zero at negative bias, because as the electron concentration increases in the semiconducting membrane, recombination eventually becomes competitive with sustained charge separation. Under such conditions, decreases in $\mathbf{k}_{sd}$ produce less recombination at a given electrode potential and, therefore, produce a negative shift in the $J-E$ curve.

With a nonzero value of the direct-reduction rate constant ($\mathbf{k}_{sc} = 1.0 \times 10^{-5}$, curves with filled symbols), an inflection point in the $J-E$ characteristics is produced when $\mathbf{k}_{sd} > 10$. The inflection point becomes more prominent, and appears at more positive bias, as the recombination rate constant ($\mathbf{k}_{sd}$) increases. When $\mathbf{k}_{sd} = 100$ (corresponding to $k_{sd} \approx 10^{-12}$ to 10^{-11} cm^3 s^{-1}), the curve with $\mathbf{k}_{sc} = 1.0 \times 10^{-5}$ (the filled down-triangle symbol) almost overlaps with the corresponding curve of zero direct-reduction rate (open down-triangle) for $E > -0.2$ V relative to the short-circuit potential of the photoelectrode.

This behavior is a consequence of the potential dependence of the recombination current relative to the potential dependence of the direct-reduction current. At sufficiently large values of $\mathbf{k}_{sd}$ (>10) or sufficiently small values of $\mathbf{k}_{cd}$ (<100), negligible photocurrent yield is obtained until relatively positive potentials are applied to the photoelectrode. At these potentials, the direct-reduction current is very small and the $J-E$ curve is dominated by the photocurrent. As the potential becomes more negative, the direct-reduction current becomes larger and dominates the total current. In this regime, the light-induced portion of the current is potential dependent and the quantum yield for collection of light-generated charge carriers is generally less than unity. The inflection point thus indicates the potential at which the overall direct-reduction current (k_{sc}) begins to surpass the recombination current (k_{sd}). This transition effect is more pronounced, and appears at less negative bias, as the recombination rate is increased (e.g. curves for $\mathbf{k}_{sd} = 100$ in Figure 5).

E. Effects of Varying the Rate Constant for Dye Regeneration. Figure 6 depicts the effects of varying the regeneration rate constant, k_{cd}. A quantum yield of unity was assumed for injection of electrons from the excited state of the dye into the TiO_2 ($\phi_s = 1$), but the low-intensity limit was not assumed in these simulations to allow the concentration of reduced dye under illumination to be less than the analytical concentration of dye adsorbed onto the TiO_2 membrane. The parameter values were otherwise as described for the baseline scenario of Table 1.

The effect of regeneration (k_{cd}) on the $J-E$ characteristic depends on which of the electron loss pathways is dominant. As shown in Figure 5, at one asymptote, regeneration must be sufficiently rapid to compete with recombination and thereby produce a unity quantum yield for light-induced charge separation at potentials negative of open circuit. For the parameters

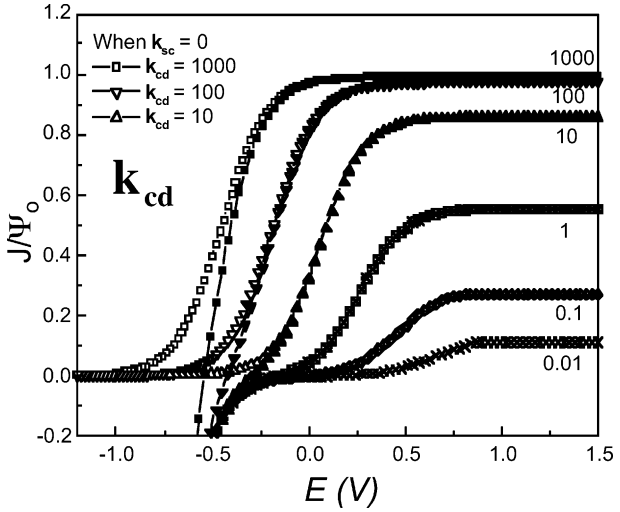

Figure 6. *J*−*E* characteristics at various values of the rate constant parameter for dye regeneration ($\mathbf{k}_{cd}$). A quantum yield for injection of $\phi_s = 1$ was assumed, but the low-intensity simplification was not used. Labels correspond to values of $\mathbf{k}_{cd}$. Curves showing the limiting behavior under the condition of no direct-reduction reaction ($\mathbf{k}_{sc} = 0$) are included for comparison and to show the origin of the inflection behavior for the curves with $\mathbf{k}_{cd}$ = 1000, 100, and 10, respectively (open symbols). Other parameters are the same as those in Figure 1.

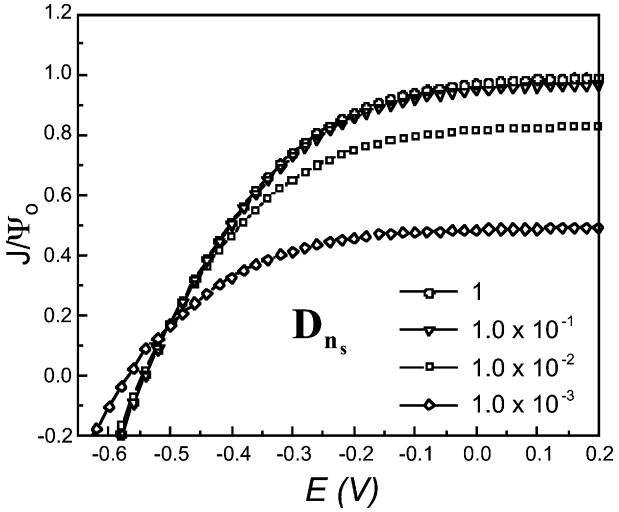

Figure 7. *J*−*E* characteristics at various values of the dimensionless diffusion coefficient parameter for electrons ($\mathbf{D}_{n_s}$). Calculations are in the low-intensity limit and under unity injection conditions ($\phi_s = 1$). Other parameters are the same as those in the baseline scenario of Figure 1.

of Table 1, this asymptote is only reached when $\mathbf{k}_{cd} > 1000$ (Figure 6). In this regime, the *J*−*E* behavior is essentially determined by the potential dependence of the direct-reduction process. For systems with smaller rates of direct electrolyte reduction, reaching this situation requires further increases in the value of $\mathbf{k}_{cd}$ (and/or decreases in the value of $\mathbf{k}_{sd}$, cf. Figure 5), so that a unity quantum yield for light-induced charge separation is obtained at even more negative electrode potentials.

The rate of recombination increases with decreasing potential while the rate of regeneration is independent of potential. The break in the *J*−*E* curves (for $\mathbf{k}_{sc} = 0$) occurs when recombination becomes competitive with regeneration. Thus, as the regeneration rate is lowered, the *J*−*E* curves shift to more positive potentials. For smaller values of $\mathbf{k}_{cd}$, recombination ($\mathbf{k}_{sd}$) competes with regeneration even at relatively positive electrode potentials. A consequence of this potential-dependent competition between recombination and regeneration is that a relatively positive potential is required to suppress recombination and reach a unity quantum yield for separation of light-induced charge carriers. Further decreases in the value of $\mathbf{k}_{cd}$ (i.e., $\mathbf{k}_{cd} < 100$ in Figure 6) result in a plateau of the photocurrent at values less than a unity quantum yield, even at very positive electrode potentials. This behavior results from the fact that regeneration is never able to compete fully with charge-carrier recombination in the membrane. Application of an increasingly positive potential to the current-collecting contact will initially increase the electron concentration gradient, thereby inducing more charge separation in the membrane and effecting a potential-dependent increase in the photocurrent. However, at sufficiently positive potentials, the concentration of electrons at the current-collecting contact becomes very small (according to the Boltzmann relationship of eq 16 in the preceding manuscript), and the electron concentration gradient is then insensitive to changes in applied potential. Under such conditions, the photocurrent exhibits a plateau that is independent of the electrode potential, with a limiting quantum yield that reflects the kinetic competition between regeneration and recombination of photogenerated charge carriers throughout the semiconducting membrane. The decrease in the current with decreasing bias is the result of increases in the rate of recombination.

F. Variation in the Diffusion Coefficient of Electrons in TiO_2. Figure 7 shows the effect of varying the diffusion coefficient of electrons in the nanocrystalline TiO_2 membrane (D_{n_s}). For values of $\mathbf{D}_{n_s} > 10^{-1}$ (corresponding to $D_{n_s} > \sim 2.0 \times 10^{-6}$ cm^{-2} s^{-1} at a membrane thickness of 10 μm), an upper-bound limit is reached beyond which further increases in D_{n_s} value have no effect on the *J*−*E* characteristics. For lower values of $\mathbf{D}_{n_s}$ (with the other parameters of the baseline scenario), the photocurrent reaches a plateau value with a quantum yield for current collection less than unity.

In the high $\mathbf{D}_{n_s}$ limit, electrons diffuse through the membrane on a time scale that is much shorter than the one describing their formation and recombination. Fick's law therefore implies that the electron concentration gradient is relatively small throughout the membrane. Under these conditions, electrons generated essentially anywhere in the membrane are readily collected at the current-collecting contact. In contrast, at very small values of $\mathbf{D}_{n_s}$, the electron concentration increases due to the increased residence time of electrons in the membrane. Because the rate of recombination is a function of the electron concentration whereas the rate of charge-carrier generation is independent of the electron concentration, the local rate of recombination can surpass the local rate of charge-carrier formation. At such small values of $\mathbf{D}_{n_s}$, even if the electron concentration at the current-collecting contact is very small, the low mobility of the electrons produces high electron concentrations away from the electrode. Consequently, local recombination exceeds local charge-carrier generation somewhere in the membrane. Once this condition is attained, the collection efficiency does not change as the bias is increased, because the gradient of the electron concentration will be negative at this point. Electrons are thus driven by diffusion away from the current-collecting contact. In this regime, the photocurrent reaches a plateau that is independent of applied potential but represents a quantum yield of less than unity for collection of light-induced charge carriers, as shown in Figure 7 for $\mathbf{D}_{n_s} < 10^{-2}$. An additional aspect of a very small value for $\mathbf{D}_{n_s}$ is that the overall electron flux ($\mathbf{D}_{n_s}(d\mathbf{N}_s/dX)_{X=0}$) decreases even though the concentration gradient at the current-collecting contact, ($d\mathbf{N}_s/dX)_{X=0}$, generally increases. This decrease in flux occurs because

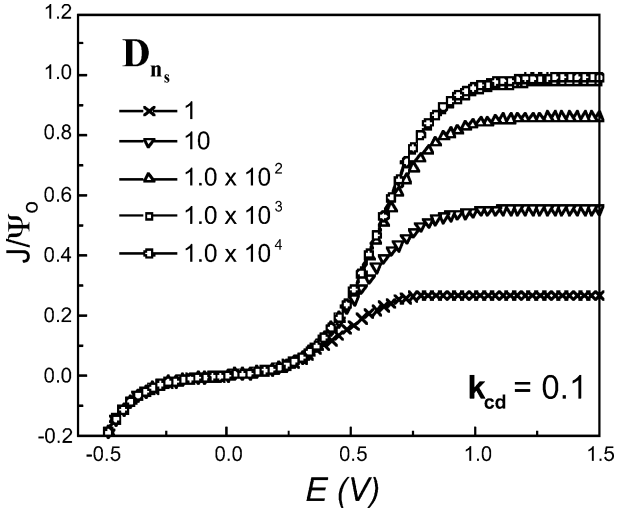

Figure 8. $J-E$ characteristics at various values of the dimensionless diffusion coefficient parameter for electrons ($\mathbf{D}_{n_s}$) under conditions where the limiting quantum yield for light-induced charge-carrier collection is less than 1.0 because recombination competes with regeneration. The curve with $\mathbf{D}_{n_s} = 1$ (×) is identical to the curve with $\mathbf{k}_{cd} = 0.1$ in Figure 6.

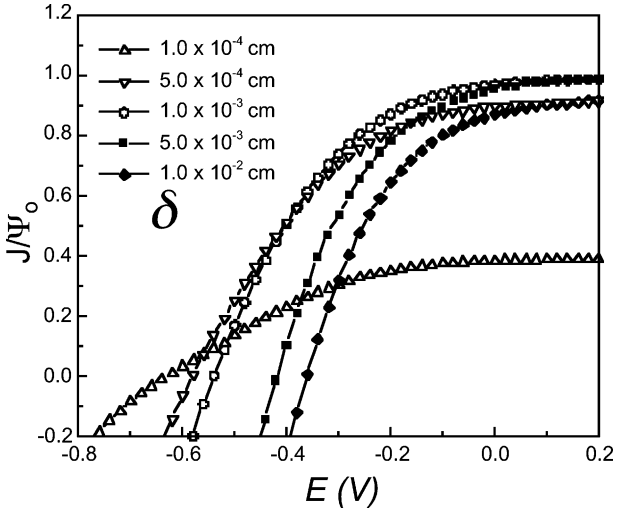

Figure 9. $J-E$ characteristics at different thicknesses (δ) of the membrane. An internal quantum yield for injection of $\phi_s = 1$ was assumed, but the low-intensity simplification was not assumed. The dimensionless diffusion coefficients ($\mathbf{D}_{n_s}$, $\mathbf{D}_{p_c}$, and $\mathbf{D}_{n_c}$) and values for the effective extinction coefficients ($\mathbf{e}_i$) were calculated according to eqs D.2.1−D.2.3 and D.4.1−D.4.6 in Table 2 in the preceding manuscript. Other parameters are the same as those in Figure 1. Curves with open symbols represent cases when $\delta \leq 10$ μm.

the increase in the concentration gradient at $X = 0$ does not completely compensate the concomitant decrease of $\mathbf{D}_{n_s}$.

In a number of systems based on dye-sensitized, nanostructured TiO_2, unit collection efficiency of light-generated charge carriers is achieved at short circuit.[14−17] This observation suggests that for the prototype system, $\mathbf{D}_{n_s}$ falls within the high diffusivity limit. The carrier mobility in the TiO_2 network is assumed to be a property of the membrane preparation and not a strong function of the identity of the adsorbed dye, so $\mathbf{D}_{n_s} = 1$ was therefore used in all of the simulations described herein unless otherwise specified.

Figure 8 shows the effects of increasing the diffusion coefficient under conditions in which recombination competes with regeneration, thereby producing a plateau value in the photocurrent for which the quantum yield for collection of light-induced charge carriers is <1 (Figure 6, $\mathbf{k}_{cd} = 0.1$). Under such conditions, increasing the value of $\mathbf{D}_{n_s}$ results in an increase in the overall flux ($\mathbf{D}_{n_s}(d\mathbf{N}_s/dX)_{X=0}$) of electrons at the current-collecting contact (Figure 7) and, therefore, produces an increase in the plateau value of the photocurrent. However, the effect is only significant in the limiting photocurrent region of the $J-E$ curve, and the potential at which the photocurrent goes to zero, due to recombination competing effectively with dye regeneration, is essentially unchanged. At a higher value of $\mathbf{D}_{n_s}$, the electron concentration is increased and is more uniform throughout the membrane. However, under these conditions, the potential-dependent recombination kinetics are highly competitive with regeneration. Thus, the lifetime of the electrons is essentially unchanged regardless of the speed with which electrons travel through the membrane. Hence, increasing the mobility of charge carriers in the semiconducting membrane can increase the limiting quantum yield in situations where recombination competes with regeneration, but such increases do not produce significant improvements in the open-circuit voltage and/or energy conversion efficiency of such photoelectrodes.

G. Variation in the Thickness of the TiO_2 Membrane, δ. The $J-E$ behavior depends on δ in a complex fashion. At a fixed value of the actual charge-carrier diffusion coefficients, changes in the thickness of the membrane produce different effective charge-carrier diffusion constants ($\mathbf{D}_{n_s}$, $\mathbf{D}_{p_c}$, and $\mathbf{D}_{n_c}$; see eqs D.2.1−D.2.3 in Table 2 in the preceding manuscript) and different effective extinction coefficients (eqs D.4.1−D.4.3 in Table 2 in the preceding manuscript). Figure 9 depicts the effects on the $J-E$ curves of such changes in δ.

In thick membranes ($\delta > \sim 10$ μm, for the chosen value of $D_{n_s} \sim 2.3 \times 10^{-5}$ cm^2 s^{-1}; Table 1), the decrease in the effective charge-carrier diffusion coefficients with increasing δ eventually results in a lowering of the limiting quantum yield, as was observed when the electron diffusion coefficient itself was decreased (section III.F). Unlike the case for decreases in $\mathbf{D}_{n_s}$ alone, however, as δ is increased, the $J-E$ curve is concomitantly shifted positively along the potential axis (cf. Figures 7 and 9) because more contact area is available for the direct-reduction reaction between electrons in the TiO_2 and oxidized species in the electrolyte solution. Hence, increasing the membrane thickness above some critical value is deleterious to the short-circuit quantum yield, open-circuit voltage, and efficiency of the photoelectrochemical cell.

In contrast, when the membrane is thinner than a critical value (e.g. $\delta < \sim 10$ μm for the diffusion coefficients chosen in the baseline scenario), the limiting quantum yield is not significantly affected by changes in δ, because the effective charge-carrier diffusion coefficients are already large enough that the system is in the high diffusivity limit. However, as the membrane thickness is decreased, less photocurrent will be produced in regions of the solar spectrum where the incident light is not fully absorbed by the adsorbed dye. Additionally, in this regime, decreases in δ produce effects that are very similar to those of decreasing the direct-reduction rate constant (k_{sc}) (Figures 3 and 4). Specifically, the entire $J-E$ curve shifts negatively as the thickness of the membrane is decreased. This is reasonable because the overall decrease in the contact time with the electrolyte is essentially equivalent to a net decrease in the rate constant (k_{sc}) per unit time (in the high diffusivity regime). Hence, in practice, the critical thickness is evaluated by examining the trade-off between photocurrent and photovoltage for a given dye-sensitized photoelectrode/electrolyte system. The diffusion coefficient of electrons in the semiconductor membrane then needs to be at, or above, the critical limit to maximize the

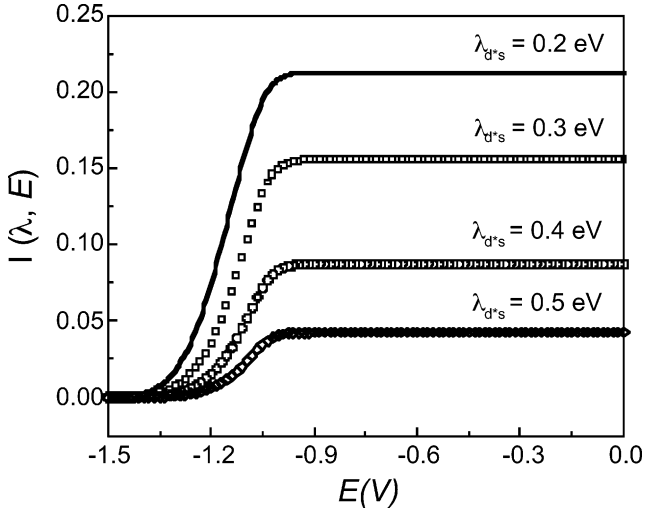

Figure 10. Injection integral, $I(\lambda_{d^*s},E)$, eq K.1.2 in Table 1 of the preceding manuscript, as a function of the applied potential at various reorganization energies. The parameters used for this calculation are $qE^{o\prime}(I_3^-/I^-) = 0.24$ eV ($=qE^{o\prime}(A/A^-)$), $qE^{o\prime}(d^{*+}/d^*) = -1.1$ eV, and $\mathbf{E}_{cb} = -0.80$ eV. The potential is measured with respect to the solution potential, $E^{o\prime}(I_3^-/I^-)$.

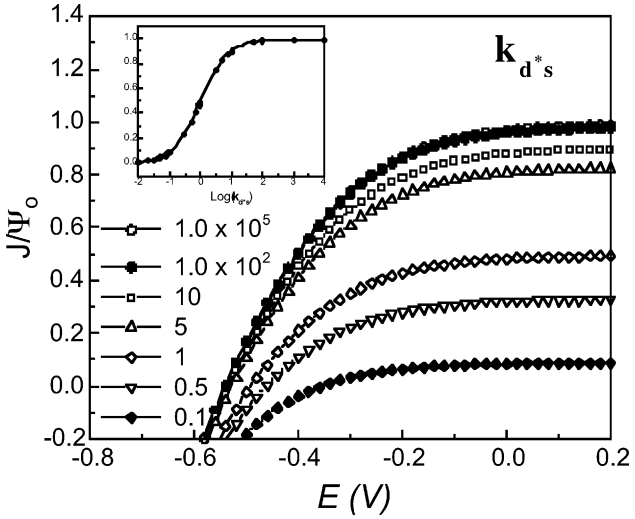

Figure 11. $J-E$ characteristics as a function of the rate constant parameter for electron injection ($\mathbf{k}_{d^*s}$) in the low-intensity limit but without assuming $\phi_s = 1$. Other parameters are same as those in the baseline scenario of Figure 1. The inset shows the current conversion efficiency measured at $E = 0.2$ V as a function of $\mathbf{k}_{d^*s}$.

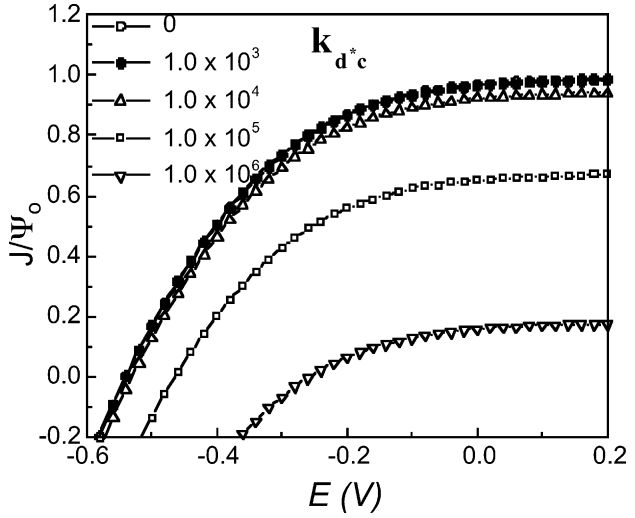

Figure 12. $J-E$ characteristics as a function of the rate constant parameter for excited-state quenching by electron transfer to oxidized species in the electrolyte ($\mathbf{k}_{d^*c}$) in the low-intensity limit but without assuming $\phi_s = 1$. Other parameters are the same as those in the baseline scenario of Figure 1.

performance of that particular dye/semiconductor/membrane thickness/electrolyte combination.

H. Effects of Decreasing the Rate Constant for Electron Injection. The expression for $\mathbf{k}_{d^*s}$ (eq K.1.1, in the preceding manuscript) predicts a decrease in the electron injection rate as the applied potential approaches the less negative of either the energy of the conduction band edge or the excited-state potential of the dye. This decrease in injection rate arises from a reduction in the number of unoccupied acceptor states that are available for electron injection when the Fermi level of the semiconductor is more negative than the conduction band edge. However, this reduction of the injection rate is generally negligible for the potential ranges of interest in typical solar cell operation (see section II.C of the preceding manuscript).[1] Figure 10 displays a numerical calculation of the "injection integral", $I(\lambda_{d^*s},E)$, as a function of applied potential at various values of the reorganization energy. The model system used for this calculation is nanocrystalline TiO_2/Ru(4,4′-dicarboxylic acid 2,2′-bipyridine)$_2$(NCS)$_2$ in $CH_3CN-I_3^--I^-$.

A significant change of the integral $I(\lambda_{d^*s},E)$ is observed only when the applied potential reaches, or becomes more negative than, the conduction band edge, at ~ -1.0 V with respect to the potential of the solution. Because the open-circuit potentials observed in many cases are ~ -0.6 V, this potential-induced reduction of the injection rate can be neglected over the normal operational potential range of interest for such systems. Qualitatively the same results have been obtained when much smaller or larger reorganization energies are used.

The effects of decreasing the rate constant for electron injection, depicted in Figure 11, are very straightforward: the limiting quantum yield decreases when nonradiative or radiative relaxation (k_d) of the excited state of the dye competes with electron injection into the semiconductor (k_{d^*s}). The unit injection yield condition ($\phi_s = 1$) was not applicable for these simulations, and instead the quantum yield was calculated from eq D.5.1 in Table 2 in the preceding manuscript.

The overall effects on the $J-E$ curves of varying $\mathbf{k}_{d^*s}$ are readily differentiated from those due to variation of $\mathbf{k}_{cd}$. At $\mathbf{k}_{d^*s} \approx 1.0 \times 10^2$, an upper-bound limit of the $J-E$ behavior is reached, above which no changes in the $J-E$ characteristics are produced. At very small injection rate constants (k_{d^*s}), the limiting quantum yield for light-induced charge-carrier collection eventually approaches zero (Figure 11 inset) due to a reduction of the net injection yield (ϕ_s) by competition from decay processes of the excited state of the dye (eqs D.3.4 and D.5.1 in Table 2 in the preceding manuscript). However, as depicted in Figure 11, the overall $J-E$ curves are always diodelike in behavior, regardless of the value of the limiting quantum yield. This is in contrast to the positive shift in the $J-E$ curves, and concomitant production of an inflection point, that accompanies smaller values of $\mathbf{k}_{cd}$ (Figure 6).

I. Effects of Excited-State Quenching by Electron Transfer to Oxidized Species in the Electrolyte. It is also possible that the excited state of the dye is competitively quenched by electron transfer to the oxidized species of the redox couple in the electrolyte solution. This situation is captured in the simulations by variation of $\mathbf{k}_{d^*c}$, as shown in Figure 12. Again, at sufficiently large values of the quenching rate constant, the limiting quantum yield decreases from unity, as was observed in Figure 11 for a slow electron injection process.

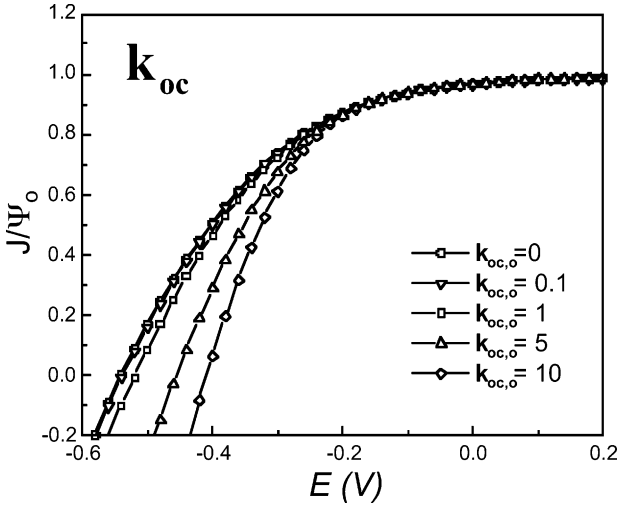

Figure 13. $J-E$ characteristics showing the effect of variation in the rate constant parameter for the leakage current ($\mathbf{k}_{oc,o}$), calculated in the low-intensity limit and with $\phi_s = 1$. Other parameters are the same as those in the baseline scenario of Figure 1.

Defining an "effective pseudo-first-order equivalent" rate constant, k'_{d^*c}, by multiplying by a concentration factor so that $k'_{d^*c} = k_{d^*c}p_c^\circ$ yields a quantity that can be compared directly to the injection rate constant (k_{d^*s}). A value of the second-order rate constant (k_{d^*c}) of $\sim 1.0 \times 10^{-10}$ cm^3 s^{-1}, and the equivalent pseudo-first-order rate constant (k'_{d^*c}) of $\sim 6.0 \times 10^{10}$ s^{-1}, corresponds to $\mathbf{k}_{d^*c} = 1.0 \times 10^5$, which is comparable to the injection rate constant parameter assumed in this study, $\mathbf{k}_{d^*s} = 1.0 \times 10^5$. In this situation, the competition from decay of the excited state can be ignored (k_d being $\sim$5 orders of magnitude smaller than the injection rate constant), and the quenching by the electrolyte, k_{d^*c}, is responsible for the decrease in the quantum yield. The value for the upper-bound limiting $J-E$ curve can be identified as $\mathbf{k}_{d^*c} = 1.0 \times 10^3$ for the parameters chosen in the baseline scenario. As is the case for decreases in $\mathbf{k}_{d^*s}$, competitive quenching of the dye excited state can be readily distinguished from decreases in the rate of dye regeneration, because the former produces $J-E$ curves that are always diodic in character, whereas the latter produces positive shifts, and concomitant formation of inflection points, in the $J-E$ behavior (Figure 6).

J. Effects of Variation in Leakage-Current Rate. Figure 13 demonstrates the effect of the $\mathbf{k}_{oc}$ parameter. This corresponds to a leakage current that is present under illumination even at open circuit. This process provides an electron loss route at the conducting substrate that is directly exposed to the contacting phase through the porous TiO_2 layer. Because k_{oc} itself contains a bias dependence (see eqs K.6.1 and K.6.2 in Table 1 in the preceding manuscript), the constant term is defined for convenience as $k_{oc,o}$. The corresponding dimensionless parameter, $\mathbf{k}_{oc,o}$, is defined in parallel with eq D.3.6 in Table 2 in the preceding manuscript. Assuming that the relative fraction of the substrate area exposed to the contacting phase (f_A) is 10^{-3} (because the active area of a 10 μm thick TiO_2 membrane is approximately 10^3 higher than its projected area), $\mathbf{k}_{oc,o} = 1$ corresponds to $k_{oc,o} \approx 0.1$ cm s^{-1} when the same value of K_I is used as defined above (i.e., $[K_I/(p_c^\circ n_c^\circ)]^{1/2} = 1$). Nonzero values of $\mathbf{k}_{oc}$ reflect the loss of electrons from uncoated areas of the conducting substrate (SnO_2) by recombination with holes in the contacting phase.

Under this set of conditions, electron loss due to this process is important only at sufficiently negative bias and when the rate constant is sufficiently large (i.e. $\mathbf{k}_{oc,o} > 0.1$). The numerical calculation of the integral, in eq K.6.2 in Table 1 in the preceding manuscript, indicates that the value of this integral decreases dramatically when the bias is more positive, and the effect of the electron loss process eventually vanishes at very low bias or under positive bias (not shown, but similar to the decay of the injection integral shown in Figure 10). Thus, the effect of the changes in the bias-independent part of the rate constant ($\mathbf{k}_{oc,o}$) would be seen only when the cell is at very negative biases. As a result, the effect of this parameter is readily distinguishable from that of $\mathbf{k}_{sc}$, because the change of $\mathbf{k}_{sc}$ generally causes an overall shift of the $J-E$ curves and produces a much larger change in the open-circuit potential, as discussed above. The contribution of the leakage current is generally neglected in the interpretation of the experimental $J-E$ curves because the relative surface area is very small compared to that of the semiconductor nanoparticles in the membrane. However, the relative contribution of the leakage current to the total cathodic current cannot be ignored when the relative fraction of the substrate area exposed to the contacting phase (f_A) is significant (see eq D.3.6 in Table 2 in the preceding manuscript), as is the case when the thickness of the membrane is decreased significantly (because f_A is inversely related to the thickness of the membrane; see section II.E in the preceding manuscript).

IV. Discussion

A. Classes of Reaction Rate Constants. Three distinct types of behaviors were observed in response to variation in the rate constant parameters. Parameters for the direct-reduction reaction ($\mathbf{k}_{sc}$), the reduced equilibrium constant for iodine formation ($[K_I/(p_c^\circ n_c^\circ)]^{1/2}$), recombination ($\mathbf{k}_{sd}$), and the membrane thickness (δ)[18] belong to the first category (type I). Parameters describing injection ($\mathbf{k}_{d^*s}$) and excited dye quenching by the contacting phase ($\mathbf{k}_{d^*c}$) belong to the second category (type II). These two groups are defined by the time scale of their rates, where class II parameters are in competition with the natural decay of the excited state of the dye while class I parameters are in competition with slower electron-transfer processes. Regeneration ($\mathbf{k}_{cd}$) is unique and defines a third category of behavior (type III).

Type I parameters affect the $J-E$ behavior mostly through changes in the open-circuit voltage or by changing the potential at which the current declines from the condition of $J/\Psi_0 = 1$. The overall $J-E$ curves are simply shifted either positively or negatively along the potential axis without significantly changing the overall shape of the curves. The $J-E$ curve shifts positively as the parameter value increases, and the shift is greater than 200 mV per order of magnitude change in the parameter value. A unity quantum yield for collection of light-induced charge carriers ($J/\Psi_0 = 1$) is reached at very positive potentials, except when the membrane thickness becomes larger than a critical value ($\delta > \sim 10$ μm), in conjunction with low charge-carrier diffusivities in the membrane, or when the membrane is too thin to allow full light absorption by the decreased amount of adsorbed dye.

Variation in the type II parameters primarily affects the limiting quantum yield for photocurrent production. Generally, the $J-E$ curves for these parameters show a limiting behavior in which a further increase ($\mathbf{k}_{d^*s}$) or decrease ($\mathbf{k}_{d^*c}$) of these parameter values produces no effect on the $J-E$ characteristics. The limiting photocurrent quantum yield drops significantly when the parameter value either decreases ($\mathbf{k}_{d^*s}$) or increases ($\mathbf{k}_{d^*c}$) and ultimately approaches asymptotically a limit of zero quantum yield, but the $J-E$ curves are still diodelike in form.

Parameters for the leakage rate constant ($\mathbf{k}_{oc}$) and the diode quality factor (f) behave quite similarly, though the variation

in the $J-E$ behavior is more pronounced upon change of the latter. Unlike the other rate constant parameters, $\mathbf{k}_{oc}$ includes a bias dependence (Figure 13). This causes a weighting effect at different bias values and makes this parameter behave as a type I parameter at a sufficiently negative bias; however, the type I characteristic is reduced at a lower, or positively biased, condition.

The dimensionless diffusion coefficient of electrons ($\mathbf{D}_{n_s}$) in the semiconductor membrane shows mixed responses of both type I and II characteristics. Decreasing the value of this parameter decreases the limiting photocurrent quantum yield (type II) but concomitantly shifts the open-circuit potential negatively (type I). For purely type II behavior, the open-circuit potential would have shifted to more positive values. The behavior occurs because, at low diffusion coefficients, electrons stay longer in the membrane before they are collected at the conducting current-collecting contact ($X = 0$). The enhanced residence time causes an increase of the electron concentration in the membrane. This has the same net effect as decreasing the rate constant for direct reduction (k_{sc}) at a given thickness of the membrane (type I) and accounts for the negative shift of the open-circuit potential at smaller values of $\mathbf{D}_{n_s}$.

The regeneration rate constant parameter ($\mathbf{k}_{cd}$) is unique in its effects on the $J-E$ behavior, and it defines the type III category. Decreasing $\mathbf{k}_{cd}$ initially produces a positive shift in the $J-E$ curves, while further decreases in $\mathbf{k}_{cd}$ additionally produce a decrease in the limiting quantum yield for photocurrent flow. The rate of recombination is dependent on the applied potential, but the rate of regeneration is independent of the applied potential. Hence, if recombination is competitive with regeneration in the limiting photocurrent region, recombination becomes increasingly dominant as the photoelectrode potential is made more negative and consequently the photocurrent decreases. This potential-dependent competition between these two rate processes produces the unique type III characteristic of $\mathbf{k}_{cd}$, allowing variation in this quantity to be easily distinguished from changes in the other parameters of the system model.

B. Charge-Carrier Transport Processes. The method described in this work differs from previous modeling efforts with respect to charge-carrier motion in that the simultaneous transport of three different charge carriers is represented. Note that this is still not the most general formulation of the problem. The transport of dye holes, which can occur by electron hopping between adjacent dye molecules, was neglected. For the conventional system, the simulations indicate that the concentration gradients for electrons and holes in the contacting phase are small (Figure 1). Hence, similar results would have been obtained by fixing these concentrations and treating only the diffusion of n_s. This conclusion is based on estimates of $\mathbf{D}_{p_c}$ and $\mathbf{D}_{n_c}$ derived from the literature and on the analytical concentrations of the redox species in the contacting phase.

When either the concentrations or the diffusivities become smaller, diffusion in the contacting phase could become a controlling feature. Minimizing the concentration of holes in the contacting phase is a viable strategy to minimize loss of photogenerated charge carriers, since the direct-reduction process limits the photovoltage in the conventional system with triiodide as the hole carrier.[19] Moreover, the concentration of triiodide should be minimized to reduce unwanted light absorption in the electrolyte. However, this approach would also require thinner cells to avoid concentration polarization losses at the counter electrode, and decreasing the membrane thickness significantly will reduce light absorption and therefore reduce the photocurrent. With regard to the effects of a reduction in charge carrier diffusivity, considerable effort is now being directed toward utilizing molten salts,[19] semisolid gels,[20,21] and conducting polymers[22] in the contacting phase as replacements for redox-active solutions. Charge-carrier diffusivities in these media are likely to be significantly smaller than those in the CH_3CN system. Decreases in the mobility of charge carriers either in the semiconducting membrane and/or in the electrolyte will eventually deleteriously affect the $J-E$ behavior of the system through increasing the electrical resistance of the photoelectrochemical cell and additionally through a decrease in the flux of light-induced charge-carrier motion due to reduced carrier movement at lower diffusion coefficient values.

C. Effects of the Direct-Reduction Process. As previously noted, the direct reduction of oxidized species in the contacting phase by electrons in the semiconductor (k_{sc}) is the process that limits the photovoltage in the conventional dye-sensitized TiO_2 system. To date, efforts to increase the photovoltage of dye-sensitized nanocrystalline TiO_2-based solar cells by replacing I_3^-/I^- with one-electron, outer-sphere redox couples have largely been unsuccessful, except for a recent report involving the behavior of a one-electron redox mediator, cobalt(II) bis[2,6-bis(1′-butylbenzimidazol-2′-yl)pyridine].[23] This lack of photovoltage increase is mostly attributed to increases in the direct-reduction rate in such systems. For example, the ferrocene$^{+/0}$ system, which has nearly the same formal potential as I_3^-/I^-, cannot be used as a mediator in a dye-sensitized cell unless the direct-reduction reaction of electrons with the oxidized redox species is reduced.[13] Thus, the redox system must be kinetically slow on TiO_2 (low k_{sc}) and on the substrate (low k_{oc}) but kinetically fast for regeneration (high k_{cd}) and rapidly reduced at the cathode.[24,25] Although the effects of interfacial electron-transfer kinetics at the cathode were not considered in this study, we note that I_3^-/I^- is especially well-suited because its exchange-current density is low on F-doped SnO_2 but rapid on metal-film (e.g. Pt) cathode materials. This is consistent with the reaction scheme used in this model, which is derived from the dissociative chemisorption of I_2 (eqs 6.1−6.3 in the preceding paper). This scheme provides a facile electron-transfer route at a platinum electrode while the electron-transfer rate at fluorine-doped SnO_2 is known to be over 5 orders of magnitude lower. Other reaction schemes are also compatible with the modeling used herein, provided that the resulting direct-reduction rate constants and concentrations of oxidized species in the electrolyte yield the same dependence of cathodic current on applied bias as that observed experimentally and simulated herein as the baseline scenario.

D. Competition between Recombination and Regeneration. The potential-dependent competition between transport, recombination, and regeneration requires a quantitative simulation model to assess the influence of various rate constant values on the $J-E$ properties of the photoelectrochemical cell. For example, a key result of the present simulations is that currently available experimental parameters determined from dynamics experiments under open-circuit conditions are apparently not capable of producing the observed photovoltage of these electrodes under typical steady-state illumination fluxes.

The experimentally observed $J-E$ curves for the nanocrystalline TiO_2-based cells sensitized with Ru(II) or Os(II) polypyridyl complexes[12] more closely resemble those for $\mathbf{k}_{sd} \leq 10$ with $\mathbf{k}_{sc} = 1.0 \times 10^{-5}$ when $\mathbf{k}_{cd} = 1.0 \times 10^{3}$ in Figure 5 (i.e., no distinct sign of inflection behavior). The observation of the distinct inflection point for the situation where $\mathbf{k}_{sd} = 10$ and $\mathbf{k}_{cd} = 100$ (with $\mathbf{k}_{sc} = 1.0 \times 10^{-5}$, filled down-triangle, Figure

1) indicates that either $\mathbf{k}_{cd}$ is underestimated or $\mathbf{k}_{sd}$ is overestimated with this choice of input parameters. Some combination of increase in $\mathbf{k}_{cd}$ and/or decrease in $\mathbf{k}_{sd}$ is required to produce a unity quantum yield for collection of light-induced charge carriers at potentials slightly negative of open circuit, so that the direct-reduction current, and not recombination, determines the position of the open-circuit potential under illumination. It is more likely that $\mathbf{k}_{cd}$ is underestimated because the value of the recombination rate constant, $k_{sd} \approx 10^{-13}$ to 10^{-12} cm^3 s^{-1}, corresponding to $\mathbf{k}_{sd} = 10$, is relatively close to the experimentally measured value, 3.0×10^{-12} cm^3 s^{-1}.[7] This observation prompted the use of a value for $\mathbf{k}_{cd}$ in the baseline scenario (Table 1 and Figure 1) that was somewhat larger than the value measured experimentally.

Another effect that requires a simulation method for quantitative analysis is the observation of a limiting photocurrent value at a quantum yield less than unity for collection of light-generated charge carriers. This behavior is commonly observed for many dye-sensitized photoelectrochemical cells but would not generally occur at crystalline semiconductor photoelectrodes, for which sufficient reverse bias could always be applied to ensure effective separation and collection at the current-collecting contact of light-induced charge carriers. At least four separate phenomena can in principle account for this observation at dye-sensitized nanocrystalline semiconductor photoelectrodes.

First, the photocurrent yield can be limited by a low electron diffusivity in the membrane (Figure 7). However, as described above, it is reasonable to assume that, for a homologous series of transition metal dye sensitizers, the mobility of charge carriers in the membrane is independent of the molecular composition of the dye. Because several nanocrystalline TiO_2 systems are well-documented to produce internal quantum yields of unity for collection of light-induced charge carriers,[12] it appears that these specific membrane compositions are in the high-diffusivity limit under such conditions.

A second possibility is that the flux of light-induced charge carriers injected into the semiconductor membrane may be significantly lower than the photon flux incident onto the photoelectrode. Two fundamentally different processes can in principle be responsible for this behavior. Either the excited state of the dye can be competitively quenched by reaction with oxidized species in the solution phase and/or the equilibrium concentration of reduced dye on the photoelectrode is not sufficient to effect significant absorption of the photon flux incident onto photoelectrode. As shown in Figures 11 and 12, such effects manifest themselves by reducing the photocurrent density (and thereby concomitantly reducing the photovoltage) without introducing an inflection point in the resulting $J-E$ curves.

A third possibility for obtaining a low limiting photocurrent density occurs when the steady-state concentration of reduced, light-absorbing, adsorbed dye is much less than the analytical concentration of dye adsorbed onto the TiO_2 photoelectrode. This situation will occur when the Nernstian potential of the electron-donating species in the contacting phase is close to, or more positive than, the Nernstian potential of the ground state of the dye (e.g. when $\Delta G_{cd} \geq 0$). In such a situation, charge equilibration between the dye and the species in the solution will tend to restore the ratio of oxidized to reduced dye to its equilibrium value. Because only light absorption by the reduced dye results in excited states that inject electrons into the semiconductor membrane, a reduction in the concentration of adsorbed reduced dye species will produce a significant decrease in the amount of the necessary light absorber and, consequently, will produce a reduced limiting external quantum yield for photocurrent flow.

A fourth possibility is that regeneration is not rapid enough to compete with recombination, as depicted in Figures 5 and 6. This situation is, however, readily differentiated from the situations discussed above that produce a reduced flux of injected charge carriers into the TiO_2. The competition between recombination and regeneration produces a distinctive effect on the $J-E$ curves, with an inflection point in the photocurrent followed by attainment of a plateau region only at very positive electrode potentials (Figure 6). Additionally, systems that display low limiting quantum yields for photocurrent flow are predicted to show even lower, potential-dependent, yields for photocurrent flow as the photoelectrode is biased negatively of the short-circuit potential.

Recent measurements on a series of dyes separated from the TiO_2 membrane by bridging ligands of various lengths are consistent with the behavior expected for systems displaying competitive quenching of the excited state.[26] The members of this series of dyes have mutually similar ground-state formal potentials and also have mutually similar formal potentials for formation of oxidized dye from the thermalized excited state of the reduced dye. Furthermore, spectroscopic measurements indicate that electron injection on all of these dye-sensitized photoelectrodes is more rapid than excited state decay and that the rates of recombination and regeneration are nearly identical for all three dyes.[26] However, the limiting quantum yields for photocurrent flow differ significantly, with the longer linkers systematically having lower steady-state quantum yields for photocurrent flow than the shorter linkers. This behavior is consistent with expectations for competitive quenching of the excited state of the dye by the oxidized species in the electrolyte, in which the competition between the rates of quenching and electron injection into the TiO_2 is a function of linker length. Hence, although the use of longer tethers may reduce recombination by the k_{sd} pathway, unless the electronic coupling in the linker is tailored appropriately, injection through such linkers may not be sufficiently rapid to preclude other deactivation pathways from deleteriously affecting the efficiency of the resulting photoelectrochemical cell.

The $J-E$ behavior for a series of Ru and Os dyes in contact with Br_2/Br^- relative to I_3^-/I^- is consistent with our simulation of a decreased flux of injected light-induced charge carriers, because the $J-E$ curves show a systematic decrease in quantum yield in contact with Br_2/Br^- relative to the current in contact with I_3^-/I^-, and photoelectrochemical cells that display very low limiting quantum yields for photocurrent flow show no inflection point in the $J-E$ behavior (Figure 6).[27] Explaining this low quantum yield solely in terms of a reduced rate constant for regeneration would require that, in contrast to the behavior of Figure 6, recombination is essentially independent of potential over the 0.8 V range between the short-circuit and open-circuit potentials. Hence, the simulations presented herein can be used to provide valuable insight into the underlying features that control the $J-E$ characteristics of a homologous series of dye-sensitized photoelectrodes.

E. Concentration Profiles for Electrons in the Semiconductor Membrane. When the applied bias is sufficiently negative, the simulations yield a peak in the electron concentration within a short distance from the current-collecting contact ($X = 0$). This peak is more pronounced as the bias becomes more negative (Figure 1). Similar concentration profiles have been suggested by Fisher et al.,[24] through the use of other models under different bias and excitation conditions. These models

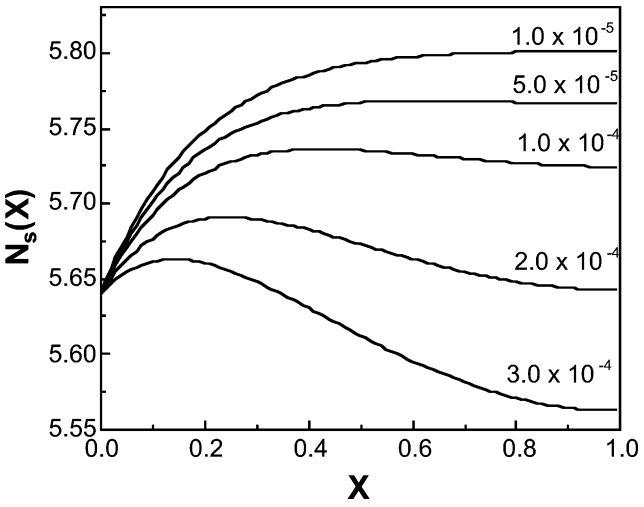

Figure 14. Concentration profiles for electrons in the semiconductor ($\mathbf{N}_s(X)$) calculated at $E = -0.2$ V. Labels correspond to values of $\mathbf{k}_{sc}$. Other parameters are the same as those in the baseline scenario of Figure 1.

produce a localized increase in the electron concentration when the rate of direct reduction is increased.[24] Figure 14 presents the results of the present model for the concentration profiles of electrons as a function of position in the membrane, at different values of the direct-reduction rate parameter $\mathbf{k}_{sc}$. These simulations also show an increase in the local electron concentration near the current-collecting contact. This behavior can be understood by comparing the bias dependence of the concentration profiles in Figure 1 with the effect of $\mathbf{k}_{sc}$ on the $J-E$ curves of Figure 3. The spatially localized increase of the electron concentration at high $\mathbf{k}_{sc}$ values has essentially the same origin as the spatially localized increase in $\mathbf{N}_s(X)$ at very negative applied potentials, because the increase of the $\mathbf{k}_{sc}$ value shifts the overall $J-E$ curve positively, being virtually equivalent to applying a more negative bias to the cell.

V. Summary and Conclusions

The set of simulations discussed herein provides insight into the operational characteristics and factors that affect the performance of dye-sensitized nanocrystalline semiconductor-based photoelectrochemical cells. Apparently, the diffusion coefficient of charge carriers in the TiO_2 under steady-state conditions is in the high-mobility limit, and relatively little improvement in $J-E$ behavior is thus predicted to result from further increases in the charge-carrier mobility for these specific types and thicknesses of the semiconductor membrane. Thicker membranes are predicted to deleteriously affect the $J-E$ behavior because the short-circuit current density will decrease unless the charge-carrier diffusion coefficient is increased concomitantly. However, even if the increase in thickness is accompanied by an increase in charge-carrier diffusivity, the open-circuit potential will decrease with increasing membrane thickness due to the increased contact area (and consequent increase in the rate of direct reduction) between the membrane and the oxidized species in the electrolyte. Hence, the film should only be thick enough to ensure that nearly all of the incident light is absorbed by the adsorbed reduced dye species. Changes in the rate of the direct-reduction reaction obviously directly affect the photovoltage by affecting the magnitude of the cathodic current flowing at negative bias of the photoelectrode, and reductions in this current are clearly beneficial to the performance of the cell. The rate constant for light-induced charge-carrier injection (k_{d^*s}) can be reduced without deleteriously affecting the cell performance only as long as injection proceeds competitively with other mechanisms for quenching of the excited state, such as oxidative quenching by the electrolyte (k_{d^*c}). Changes in the rate constants for recombination and regeneration, although coupled in the $J-E$ behavior over a certain range of potentials, are separable by examining their influence over the entire $J-E$ behavior between open-circuit and short-circuit conditions. Because of the potential-dependent nature of the recombination process, significant decreases in the rate of regeneration cannot be compensated for by concomitant decreases in the rate constant for recombination. Hence, regeneration needs to be maintained above a lower-bound value to obtain a unity quantum yield for collection of light-generated charge carriers at negative potentials relative to short circuit. Finally, the thermodynamics of the $dye^{+/0}$ system relative to the species in the electrolyte that accept and donate electrons with the dye must be sufficiently favorable to ensure that the concentration of the reduced form of the adsorbed dye under steady-state conditions is adequate to absorb fully the light incident onto the photoelectrode, or the limiting photocurrent density will be significantly reduced. The model and simulations presented herein offer a method for evaluating where a specific system of interest lies in performance space and what dynamic and thermodynamic factors ought to be manipulated to have maximal effect on improving the efficiency of the resulting photoelectrochemical energy conversion system.

Acknowledgment. The authors gratefully acknowledge the Department of Energy, Office of Basic Energy Sciences, for funding this work under Grant DE-FG03-88ER13932.

References and Notes

(1) Lee, J.-J.; Coia, G. M.; Lewis, N. S. *J. Phys. Chem. B* **2004**, *108*, 5269.

(2) Papageorgiou, N.; Grätzel, M.; Infelta, P. P. *Sol. Energy Mater.* **1996**, *44*, 405−438.

(3) Each triiodide ion supplies two holes.

(4) Janz, G. J.; Tomkins, R. P. T. *Nonaqueous Electrolytes Handbook*; Academic: New York, 1972; Vol. 1.

(5) Papageorgiou, N.; Barbe, C.; Grätzel, M. *J. Phys. Chem. B* **1998**, *102*, 4156−4164.

(6) This value is derived by integrating the photon flux in the 100 mW cm^{-2} air mass 1.5 spectrum from 1.8 to 3.1 eV. It corresponds to a maximum photocurrent density of 16 mA cm^{-2}.

(7) Kuciauskas, D.; Freund, M. S.; Gray, H. B.; Winkler, J. R.; Lewis, N. S. *J. Phys. Chem. B* **2001**, *105*, 392−403.

(8) Press, W. H.; Flannery, B. P.; Teukolsky, S. A.; Vetterling, W. T. *Numerical Recipes: The Art of Scientific Computing*; Cambridge: 1986; Vol. section 15.1.

(9) Tachibana, Y.; Haque, S.; Mercer, I.; Durrant, J.; Klug, D. *J. Phys. Chem. B* **2000**, *104*, 1198−1205.

(10) Tachibana, Y.; Moser, J.; Gratzel, M.; Klug, D.; Durrant, J. *J. Phys. Chem.* **1996**, *100*, 20056−20062.

(11) Katz, J. E.; Coia, G. M.; Lewis, N. S. In preparation.

(12) Sauve, G.; Cass, M.; Coia, G.; Doig, S.; Lauermann, I.; Pomykal, K.; Lewis, N. *J. Phys. Chem. B* **2000**, *104*, 6821−6836.

(13) Gregg, B.; Pichot, F.; Ferrere, S.; Fields, C. *J. Phys. Chem. B* **2001**, *105*, 1422−1429.

(14) Nazeeruddin, M. K.; Kay, A.; Rodicio, I.; Humphrybaker, R.; Muller, E.; Liska, P.; Vlachopoulos, N.; Gratzel, M. *J. Am. Chem. Soc.* **1993**, *115*, 6382−6390.

(15) Amadelli, R.; Argazzi, R.; Bignozzi, C. A.; Scandola, F. *J. Am. Chem. Soc.* **1990**, *112*, 7099−7103.

(16) Alebbi, M.; Bignozzi, C. A.; Heimer, T. A.; Hasselmann, G. M.; Meyer, G. J. *J. Phys. Chem. B* **1998**, *102*, 7577−7581.

(17) Nazeeruddin, M. K.; Pechy, P.; Grätzel, M. *Chem. Commun.* **1997**, 1705−1706.

(18) The effect of the variation of thickness is more complex than simply classifying it into one category (see section III.F for details). However, the classification here is largely based on the case when the effect of the concomitant changes in the "effective diffusion coefficient" is neglected, as briefly discussed in section IV.E.

(19) Papageorgiou, N.; Athanassov, Y.; Armand, M.; Bonhote, P.; Pettersson, H.; Azam, A.; Grätzel, M. *J. Electrochem. Soc.* **1996**, *143*, 3099−3108.

(20) Yanagida, S.; Kambe, S.; Kubo, W.; Murakoshi, K.; Wada, Y.; Kitamura, T. *Z. Phys. Chem.—Int. J. Res. Phys. Chem. Chem. Phys.* **1999**, *212*, 31−38.

(21) Cao, F.; Oskam, G.; Searson, P. C. *J. Phys. Chem.* **1995**, *99*, 17071−17073.

(22) Murakoshi, K.; Kogure, R.; Wada, Y.; Yanagida, S. *Sol. Energy Mater.* **1998**, *55*, 113−125.

(23) Nusbaumer, H.; Moser, J.; Zakeeruddin, S.; Nazeeruddin, M.; Grätzel, M. *J. Phys. Chem. B* **2001**, *105*, 10461−10464.

(24) Fisher, A.; Peter, L.; Ponomarev, E.; Walker, A.; Wijayantha, K. *J. Phys. Chem. B* **2000**, *104*, 949−958.

(25) Duffy, N. W.; Peter, L. M.; Rajapakse, R. M. G.; Wijayantha, K. G. U. *J. Phys. Chem. B* **2000**, *104*, 8916−8919.

(26) Kilsä, K.; Mayo, E. I.; Kuciauskas, D.; Villahermosa, R.; Lewis, N. S.; Winkler, J. R.; Gray, H. B. *J. Phys. Chem. A*, in press.

(27) Mayo, E. I.; Kilsä, K.; Freund, M. S.; Gray, H. B.; Lewis, N. S. In preparation.